International Journal of High-Rise Buildings
December 2018, Vol 7, No 4, 343-362
https://doi.org/10.21022/IJHRB.2018.7.4.343

International Journal of
High-Rise Buildings
www.ctbuh-korea.org/ijhrb/index.php

A Simplified Steel Beam-To-Column Connection Modelling Approach and Influence of Connection Ductility on Frame Behaviour in Fire

Ruoxi Shi[1†], Shan-Shan Huang[2], and Buick Davison[2]

[1]*OFR Consultants, UK*
[2]*Department of Civil & Structural Engineering, The University of Sheffield, UK*

Abstract

A simplified spring connection modelling approach for steel flush endplate beam-to-column connections in fire has been developed to enable realistic behaviour of connections to be incorporated into full-scale frame analyses at elevated temperature. Due to its simplicity and reliability, the proposed approach permits full-scale high-temperature frame analysis to be conducted without high computational cost. The proposed simplified spring connection modelling approach has been used to investigate the influence of connection ductility (both axial and rotational) on frame behaviour in fire. 2D steel and 3D composite frames with a range of beam spans were modelled to aid the understanding of the differences in frame response in fire where the beam-to-column connections have different axial and rotational ductility assumptions. The modelling results highlight that adopting the conventional rigid or pinned connection assumptions does not permit the axial forces acting on the connections to be accurately predicted, since the axial ductility of the connection is completely neglected when the rotational ductility is either fully restrained or free. By accounting for realistic axial and rotational ductilities of beam-to-column connections, the frame response in fire can be predicted more accurately, which is advantageous in performance-based structural fire engineering design.

Keywords: Component-based model, Ductility demand, Connection, Semi-rigid, Fire

1. Introduction

The importance of steel and composite beam-to-column connections has been emphasised in both full-scale fire tests at Cardington (Newman et al., 2006) and building disasters, for instance, the collapse of WTC 7 (FEMA, 2002a, 2002b). Traditionally, the connections are assumed to be able to withstand fire attack because of their lower temperature and slower heating rate compared with the structural members they are linked to. However, the above evidence has shown that the connections are actually the most vulnerable structural members under fire conditions. Connections are typically designed for the ultimate limit state at ambient temperature. But, the force scenario changes significantly under elevated temperature and becomes much more complex (Burgess et al., 2012).

Steel beam-to-column connections can be simulated using a detailed finite element modelling approach e.g. in *ABAQUS* or a component-based modelling approach in *VULCAN*, a finite element software package developed specially for structures in fire at the University of Sheffield. These approaches can provide a reasonably accurate representation of connection behaviour, but they are not efficient in computing time, especially in frame analysis where multiple connections are presented. Furthermore, the existing commercial version of *VULCAN* includes the effects of translational and rotational springs *separately*; using this approach the behaviour of steel connections cannot be simulated accurately because the interaction of the effects is not modelled. In order to combat the drawbacks of the above two modelling approaches, a simplified spring connection modelling approach was proposed in this research. The development was based on a flush endplate connection with six bolt rows and the development procedure is summarised in Fig. 1.

Conventionally, the connections in frame simulations are usually assumed to be either rigid or pinned for ease of modelling, due to the simplicity of modelling the connections in this way. In some situations, these assumptions are made to save computational and/or time costs because the existing component based connection models require extensive computational and time costs. The simplified spring connection modelling approach proposed and validated in this research can provide an accurate and reliable way to include both the axial and the rotational ductilities in frame analysis much more efficiently.

†Corresponding author: Ruoxi Shi
Tel: +0044-7734395114
E-mail: ruoxi.shi@ofrconsultants.com

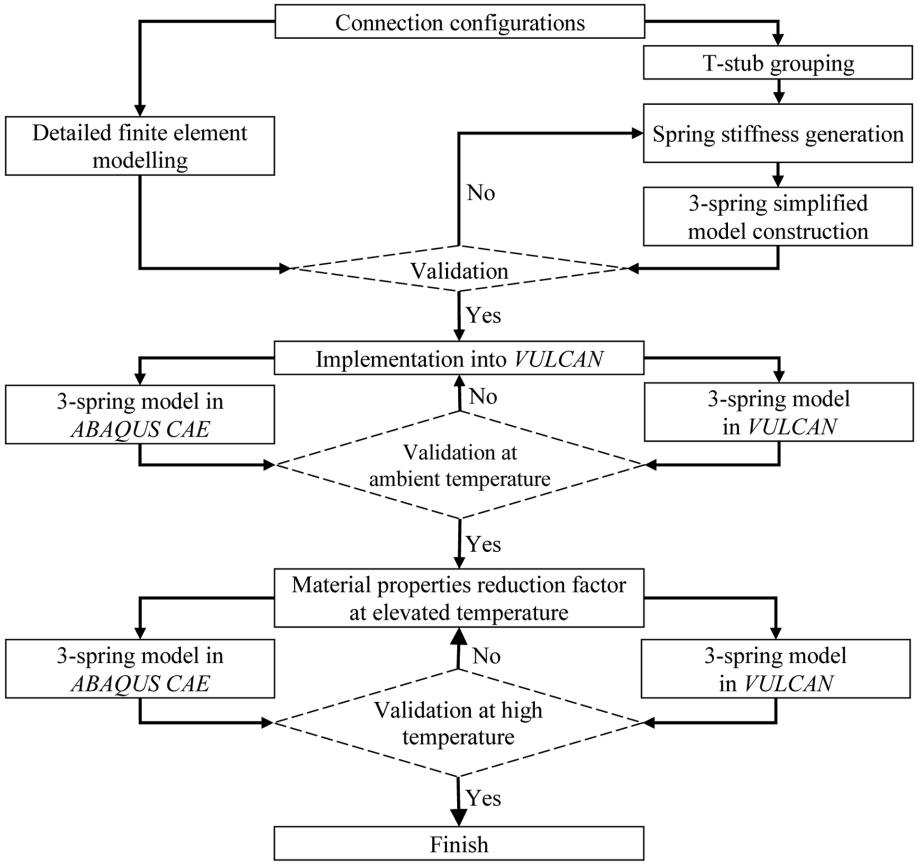


Figure 1. Development procedure of the proposed simplified spring connection modelling approach.

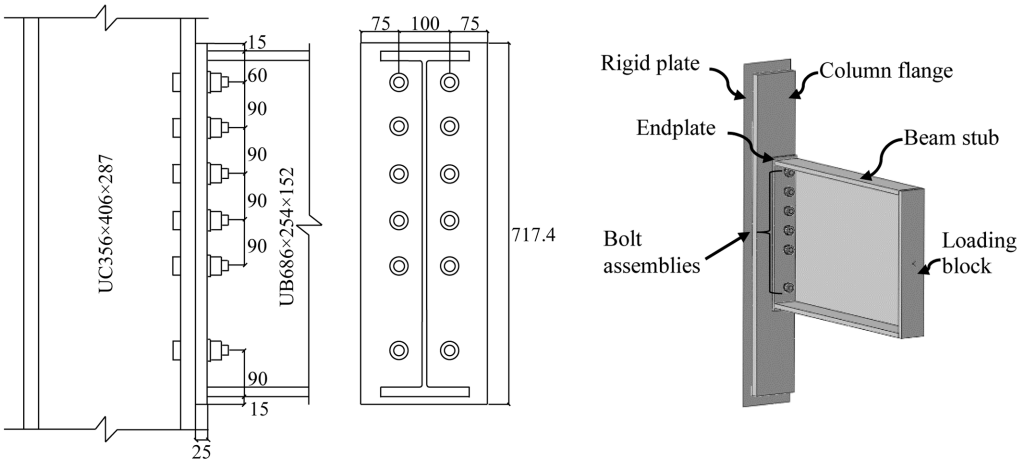
The proposed pre-processing steps using FEM to generate spring characteristics are considered to be 'simplified', compared to the detailed global frame analysis, which requires detailed FEM of each connection. The proposed approach will require pre-processing once for each type of connection, therefore, eliminating the need for repeating the detailed FEM of each connection in a frame analysis. Analytical calculation of spring characteristics was not considered in this research as relatively more accurate spring characteristics, generated via FEM, were preferred as a starting point of this approach. The development of analytical models could be considered in the future. With the proposed simplified connection modelling approach, two sets of investigations have been conducted to demonstrate the importance of incorporating connection axial and rotational ductilities in frame analysis. A set of 2D internal steel frame models with varying beam spans, from a relatively short length (6 m) to long-span (18 m), have been studied first. Next, a range of 3D composite frame models with various secondary beam spans has been conducted to include the effect of the concrete slab and composite action. This study provides an insight into frame response with more realistic, ductile connection models compared with traditional rigid or pinned choices.

2. Development and Validation of a Simplified Spring Connection Model for Realistic Sized Connections

2.1. Model development

2.1.1. Connection Configurations

A standard flush endplate connection for a realistic sized long-span (i.e., 18 m) steel frame was created and its detailed geometry information is shown in Fig. 2(a). The endplate was in structural steel grade S275 as recommended in Joints in Steel Construction: Moment-resisting Joints to Eurocode 3 (UK Connections Group, 2013). All other steel sections were also in grade S275 to simplify the input parameters. A UB686×254×152 section was used for the beam while a UC356×406×287 was used for the column. In total six rows of M24 structural bolts were adopted, again as recommended in practice (UK Connections Group, 2013). The chosen property class of bolts was 12.9 instead of the recommended 8.8 in order to ensure Failure Mode 2 (bolt fracture with endplate yielding) which provides the most ductility. (This was helpful at this stage so that both the behaviour of the bolts and endplate can be validated in the following studies.) The length of the beam stub is assumed to be 1.0 m and the height of the column



(a) Connection geometry (b) 3D model in *ABAQUS*

Figure 2. Flush endplate details.

is 1.5 m. The connection can be loaded axially, rotationally, or in a combination of both. The axial resistance of the connection was calculated to be 2284 kN in accordance with recognised design practice (UK Connections Group, 2013).

2.1.2. FEA Model of the Connection

A 3D model of the connection (Fig. 2(a)) was constructed in the finite element package *ABAQUS*, as shown in Fig. 2(b). Due to the symmetry of the connection about its vertical axis, only half of the connection was simulated thus saving computational time. Only the column flange was modelled rather than the entire column section. This is because when compared to the beam section, the column section was very stiff thus its deformation can be neglected. The bolt assemblies were modelled as one integrated element (thread stripping was neglected) comprising a bolt head, a bolt shank, a washer and a nut. The threads were not included in this simulation to save computational time and the unthreaded bolt shank size was calculated based on ISO 898-1 (BSI, 2013) and BS 3643-1 (BSI, 1981). Both solid (C3D8R) and shell (R3D4) elements were used in this simulation. For both the beam stub and the column, S275 structural steel was used. Material properties were adopted from the Eurocode 3 (CEN, 2005a). M24 property class 12.9 bolt assemblies were used for the six bolt rows in the proposed flush endplate connection. As each bolt assembly was modelled as one integrated element, identical material properties were used across each assembly based on ISO 898-1 (BSI, 2013).

Contact elements were adopted to accommodate complex interactions between parts. General surface-to-surface contact has been selected with 'Penalty' friction formulation and a friction coefficient of 0.3. Pressure-overclosure was set to 'hard' contact with 'separation after contact' allowed. The above contact elements were applied to five surface groups shown in Fig. 3: column flange – bolt heads; column flange – bolt shanks; column flange – endplate; endplate – bolt shanks and endplate – washers. The Explicit Dynamic Solver was adopted to help overcome convergence problems with multi-surface contacts in this simulation. Two types of constraints were used: 'Tie' and 'Rigid body'. 'Rigid body' constraint was applied to the loading block only. 'Tie' constraints were applied to the

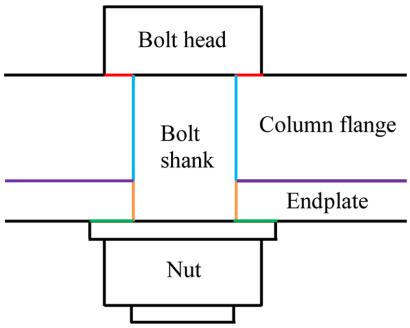


Figure 3. Contact surface groups.

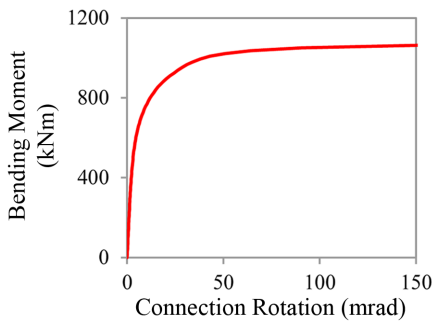
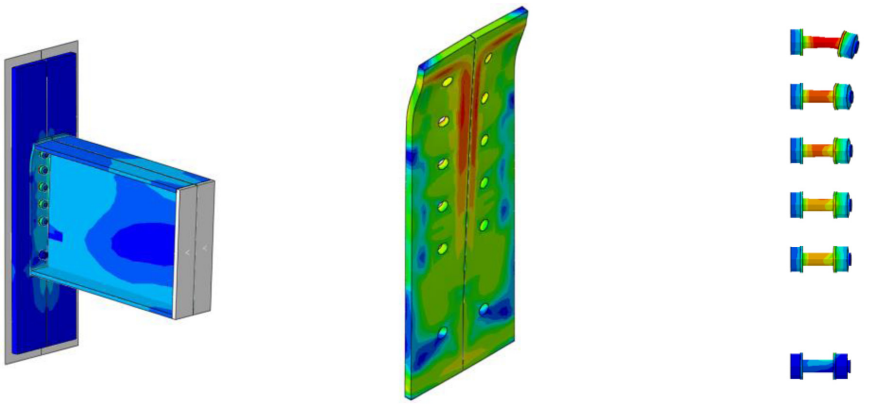


Figure 4. Connection rotational behaviour.



(a) Full connection (b) Endplate (c) Bolt rows

Figure 5. Connection deformation.

three part groups: column flange – rigid plate; beam stub – endplate and beam stub – loading block. Geometrical symmetry of the connection was represented in the model by assigning axial boundary conditions to the plane of symmetry through the centre of each part. These parts consist of the column flange, the endplate and the beam stub. The rigid plate was restrained both axially and rotationally to mimic the rest of the column.

From the simulation with a mesh size of 10 mm, chosen based on the results of a mesh sensitivity check (except for the beam stub and loading block which used 30 mm), the maximum bending moment the connection resisted was 1064 kNm and its rotational behaviour is shown in Fig. 4. The deformation shapes (Fig. 5) were as expected in terms of global deformation and localised deformation. The above results were used to validate the model developed.

2.1.3. Spring Characteristics Generation for T-stubs

In order to create the proposed simplified spring connection model, the connection was divided into 3 T-stubs to be modelled separately to generate corresponding spring force-displacement characteristics. This step involves (1) grouping multiple bolt rows into single T-stubs and then (2) conducting finite element modelling on each T-stub to generate the desired spring stiffness curve.

To make sure grouping was conducted correctly for the tensile bolt rows, a detailed connection model was loaded under bending moment only to investigate the force-displacement response of each tensile bolt row. It can be seen from Fig. 6 that bolt rows 2 to 5 behaved very similarly under pure bending while bolt row 1 was stiffer and stronger than all of the rest. This was caused by the beam top flange within the zone of bolt row 1. When the connection was loaded, forces passed from the beam to the endplate through the welds, which were modelled as 'tie' constraints. The beam top flange brought extra stiffness to the bolt row, thus the difference shown in Fig. 6. Therefore, the whole connection was divided into three T-stubs and is illustrated in Fig. 7.

The force-displacement curves of the T-stubs were gen-

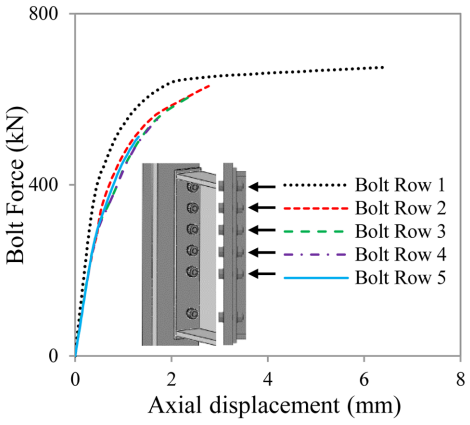


Figure 6. Tensile bolt rows under pure bending.

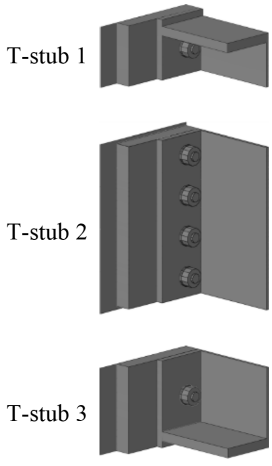


Figure 7. T-stub grouping configurations.

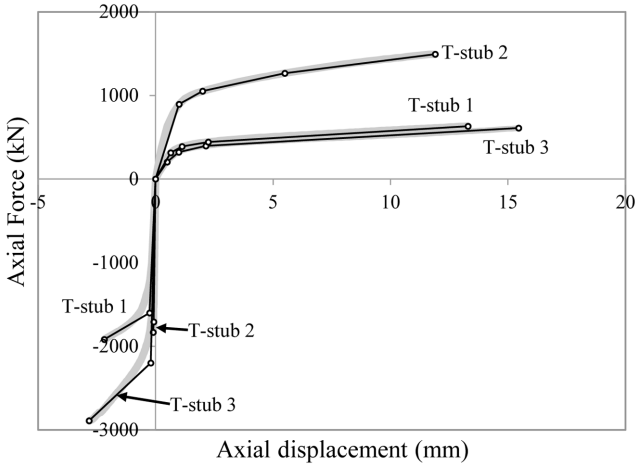


Figure 8. T-stub force-displacement curves.

erated by loading them under pure tension and pure compression. Each case was modelled until any element reached 0.20 strain. Force-displacement curves both in tension (positive) and compression (negative) for the three T-stubs are shown in Fig. 8. To satisfy the input requirement of *VULCAN*, all curves in the tensile region have been converted into 5-node multi-linear curves, while in the compressive region they have been converted into 3-node bi-linear curves. When the T-stubs were in tension, it can be noticed that T-stub 1 and T-stub 3 have very similar behaviour, this is caused by the fact that they have almost identical geometry. Coming to the compressive region, it can be noticed that although having almost identical geometry, results of T-stub 1 and 3 are apart. Compressive behaviour of T-stubs is controlled by the compressive length (the length of column web in compression in these models), thus T-stub 3 has a higher compressive capacity than T-stub 1. However for T-stub 2, even though it has the longest compressive length, without the benefit of the contribution of the beam flanges its compressive capacity is lower than the other two. Data from Fig. 8 was implemented into *VULCAN* research version in order to capture the complexity of a detailed whole connection model in a much more simplified spring model.

2.2. Model Validation

2.2.1. Validations of the Simplified Spring Model against Detailed Finite Element Simulation

An *ABAQUS* finite element model was built to validate the simplified spring approach proposed illustrated in Fig. 9. The three components of the connection were represented by two outer springs, each composed of a tensile T-stub and a compressive T-stub with different lever-arms based on the configuration of the connection, together with a central component which was a tensile T-stub. Each of the outer springs utilised only one of its pair of T-stubs at any time, depending on the sense of its force. These springs were attached to two panels; representing the column web (Panel 1) and the beam end cross-section (Panel 2). Both panels were modelled as rigid plates to ensure no deformation occurs on them, so that they could act solely as load distributors. The distance between them was set to be 50 mm, which allowed the springs to deform into the compressive region if they needed to. The whole model was fully fixed at Panel 1, while Panel 2 was free to move horizontally and to rotate. The positions of the top and bottom tensile springs were in-line with the first and the last bolt rows respectively, while the middle tensile spring was located at the horizontal centreline of T-stub 2. The two compressive springs were located at the centrelines of the beam's top and bottom flanges. The top compressive spring represents the beam top flange in compression, which might occur in certain scenarios. For instance, during initial heating, the thermal expansion of a heated beam, restrained by adjacent colder structure, could induce significant compression in the beam-to-column connection, which is mainly taken by both the top and bottom flanges of the beam. The compression springs are switched off when they are subject to tension.

The model was then loaded by an axial tensile force, F_T, and/or a bending moment, M, which was applied to Panel 2, to generate a force-displacement curve to be compared with detailed connection *ABAQUS* simulation results presented in Section 2.1.2. By constructing connection models in this manner, rotational behaviour of the connections is generated as a result of combinations of translational springs. This modelling method can provide more realistic simulation of the connections compared with modelling the connections using linearly connected axial and rotational springs.

The comparison against the detailed finite element model result presented in Section 2.1.2 is shown in Fig. 10. It can be seen that good agreement was reached.

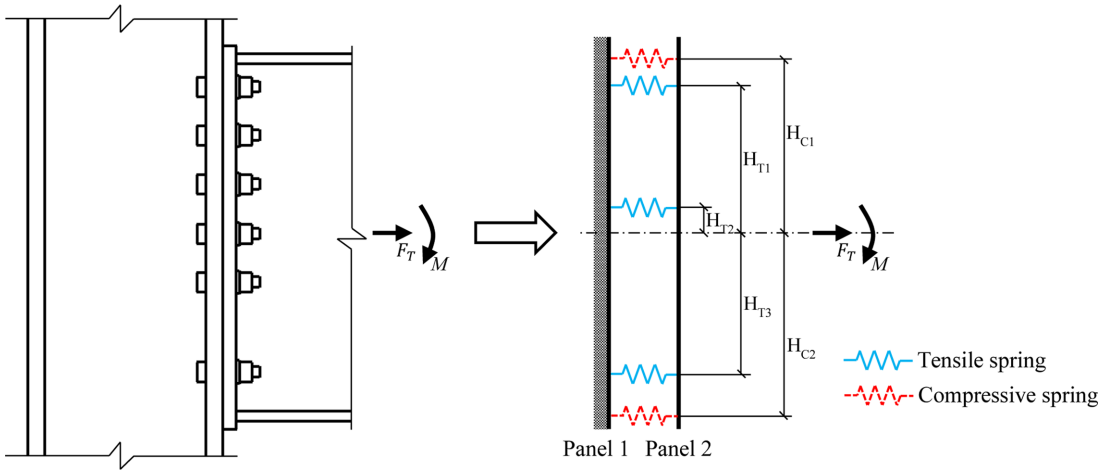


Figure 9. A connection transformed into a simplified spring connection model.

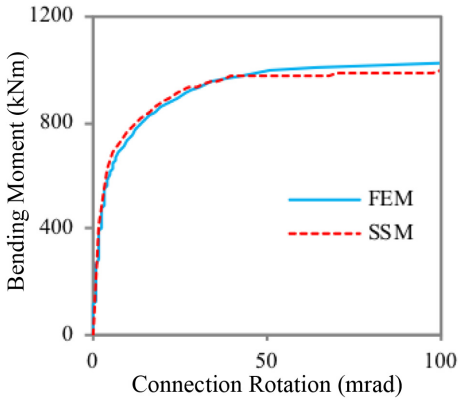


Figure 10. Simplified spring model (SSM) validating against FEM.

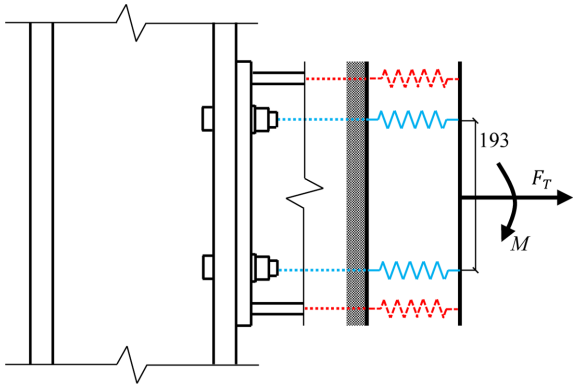


Figure 11. Simplified spring model transformation.

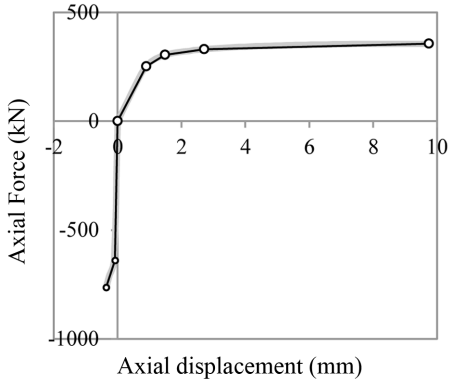


Figure 12. T-stub force-displacement curves.

2.2.2. Validation against Connection Tests by Simões da Silva et al. (2004)

Bending moment is often considered to be the main loading that affects the behaviour of steel beam-to-column connections. However, an increasing number of studies on the effects of axial force have confirmed that the presence of axial load can greatly impact on the behaviour of the joints under certain scenarios and therefore cannot be neglected (Simões da Silva et al., 2004). An experimental study of the effects of combined bending moment and axial force on flush and extended endplates has been conducted at the University of Coimbra (2004). This study highlighted that axial force can affect the connection's rotational stiffness and capacity. The test results have been utilised here to validate the proposed simplified spring model for flush endplate connections. The size of the sections (IPE240 and HEB240) and the connections are not ideal because the simplified spring connection model was developed for use with larger sections. However, due to the lack of test data on combined loadings conditions (axial force and bending moment) on long-span structures, this group of tests was chosen for validation. The specimens were loaded under various levels of constant tensile or compressive axial force expressed as a percentage of the beam plastic resistance, N_{pl}, followed by a clockwise bending moment up to failure. Three tests were selected to vali-

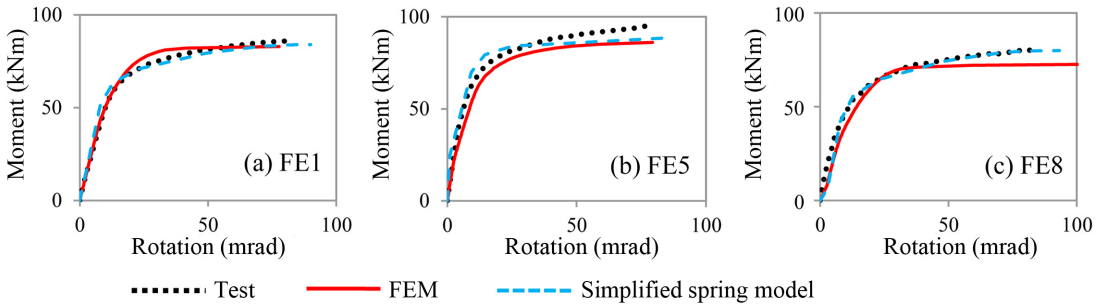


Figure 13. Validation results of FE1, FE5 and FE8.

date the proposed model: FE1 (no axial force); FE5 (20% N_{pl} in compression) and FE8 (10% N_{pl} in tension).

Due to symmetry of the connection, it has been separated into two identical T-stubs, only half of which has been modelled. The locations of the springs are as shown in Fig. 11. Force-displacement curves for this T-stub in both tension and compression are shown in Fig. 12.

Validation results are presented in Fig. 13 against the FE models and the test results. It can be seen that for all three tests, the simplified spring model can provide reasonably close results compared to both the experimental results and the detailed finite element modelling results. Therefore, the proposed simplified spring approach can be used to model steel beam-to-column connections under pure bending moment combined with tensile or compressive axial force.

2.3. Integration of the Connection Model into Global Frame Analysis

2.3.1. Existing Connection Model

A spring connection model was created by Sun et al. (2015) in the research version of the finite element software *VULCAN*. This approach was used to simulate ductility of two types of steel beam-to-column connections and thus investigate their impact on the entire frame under elevated temperature. The simulations were conducted on two-dimensional multi-storey frames with assumptions made on restraints from adjacent frames and slabs. As the characteristics of each type of connections vary, the stiffness of springs was defined to reflect these differences in assumptions. Each connection model is made up of five springs, of which three are tensile springs, and the other two are compressive springs, as illustrated in Fig. 14. Each tensile spring consists of three components, which are defined by their force-displacement characteristics entered by users. The overall stiffness of each tensile spring is then calculated as for components connected in series. The current version of the model only allows the same characteristic for each component of a certain type (column flange, bolt or endplate), and therefore the axial characteristics of the springs are identical. The rotational stiffness of the whole connection is a result of the combination of the axial springs. This model is capable of modelling frames containing whole beams with connections on both ends of the beams. With this existing connection model, previously generated T-stub force-displacement relationships (see 2.1.3) can be implemented into *VULCAN* with adjusted lever arms for modelling of different types of connections. Due to the limitation of the above spring connection model that all three of the tensile springs are identical, there was a need to modify the existing code to implement the simplified spring connection model into

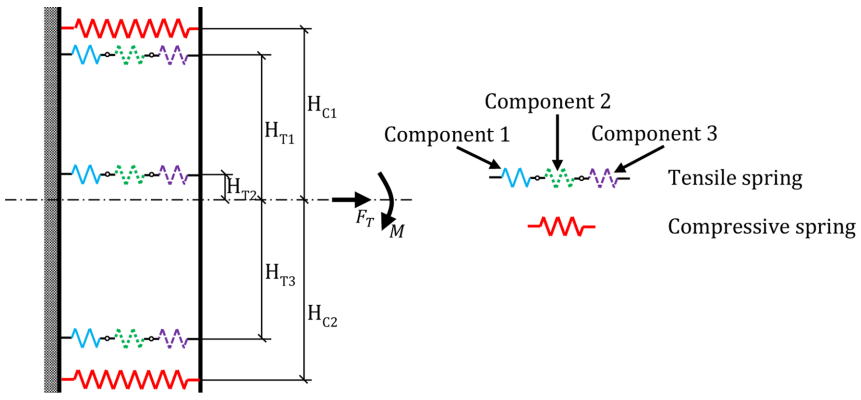


Figure 14. Spring connection model proposed by Sun et al. (2015).

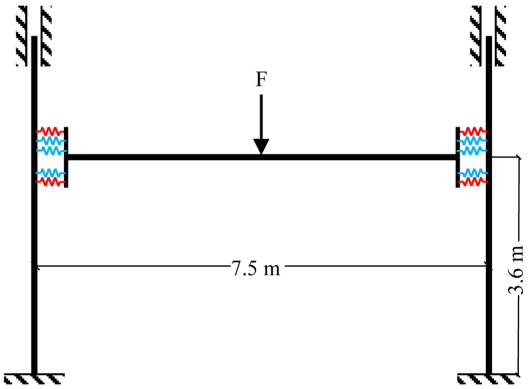


Figure 15. 2D Frame in *VULCAN* & *ABAQUS*.

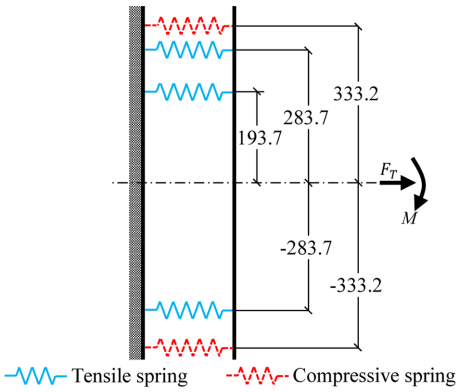


Figure 16. Simplified spring connection.

VULCAN. In effect, the spring characteristics were taken directly from full T-stub assemblies, and so it was unnecessary to consider the three components individually. To implement this, one component of each spring was selected to represent the T-stub, and the other two components were set to be very stiff and strong. Since the local conditions around the outer and middle springs differ, different stiffnesses can be assigned to them according to location. With the modifications described above, the simplified spring connection model was implemented into *VULCAN*.

2.3.2. Validation at Ambient Temperature

Fig. 15 presents a 2D rugby goalpost frame used for validation of the simplified spring connection *VULCAN* model against the *ABAQUS* spring model. The beam span and elevated height of the frame were 7.5 m and 3.6 m respectively, and its section information and material properties were the same as described in 2.1.2. The column bases were fully fixed while the tops were only allowed to move vertically, to mimic the restraint provided by the upper structure. A vertical point load, F = 1500 kN, was applied at the centre of the beam. Fig. 16 represents the details of the spring model used for beam-to-column connections on both ends of the beam. A similar model was also produced in *ABAQUS* to be used as the control results, which has been validated previously in 2.2.1.

As illustrated in Fig. 17, results produced by *VULCAN* and *ABAQUS* have a good correlation. It shows that the proposed simplified spring connection model is robust and can be used to model flush endplate connections at ambient temperature.

2.3.3. Validation at Elevated Temperature

The same models as in 2.3.2 were adopted, with changes made on temperature data from under ambient temperature to in fire conditions. The frame was assumed to be heated in ISO 834 standard fire (ISO, 1999). The model frame in *ABAQUS* was loaded up to desired level first and then heated up to match *VULCAN*.

The heating process was achieved in *ABAQUS* by adding a pre-defined temperature field and in *VULCAN* by adding a temperature data block in its input file. The temperature profiles with reduction factors for the frame elements are: beam (flange-web-flange, 0.8-1.0-1.0); column (uniform, 0.7) and connection (uniform, 0.7). These reduction factors were then applied to ISO 834 standard fire curve to generate temperature profile for each element. The beam was heated directly from the bottom flange, thus

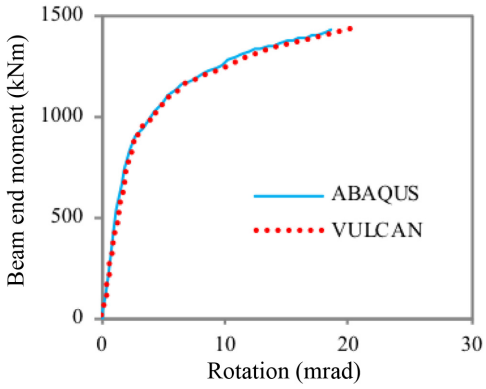


Figure 17. Validation of the simplified spring model at ambient temperature.

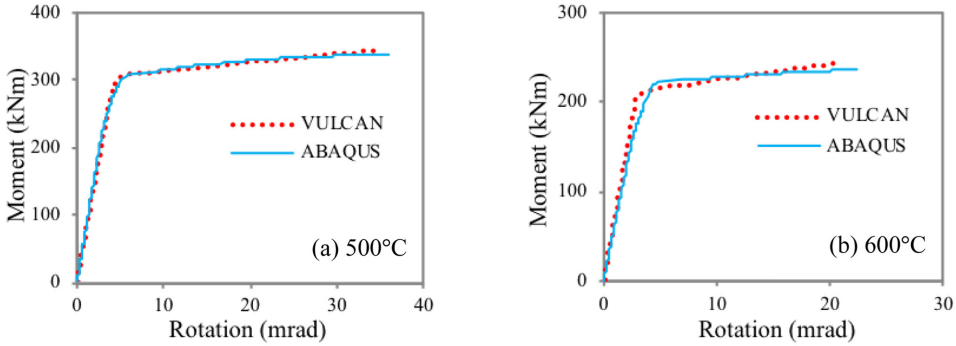


Figure 18. Validation of the simplified spring model in VULCAN and ABAQUS at elevated temperature.

the temperature of the bottom flange and web were assumed to be the same as the fire temperature. The top flange, on the other hand, was assumed to be slightly cooler due to the presence of the concrete slab. The columns are normally protected, thus a reduction factor of 0.7 was applied to the fire temperature. The connection was assumed to be the same temperature as the columns because normally connections are protected and due to its complex composition, it should heat up more slowly than bare steel. *VULCAN* research version is capable of dealing with the spring stiffness degradation with increasing temperature automatically; hence the deduction in stiffness and strength of the connections can be simulated.

550°C is commonly regarded as the 'failure temperature' for structural steel as the material yield strength is reduced to about 60% of that at 20°C. Therefore two temperatures at 500°C and 600°C were chosen for the elevated temperature validation. As the moment capacity of the connections reduces with increasing temperatures, the point loads in these two models were set at 1500 kN for the 500°C case and 1000 kN for the 600°C case.

The validation results of the proposed simplified spring approach against *ABAQUS* simulation are represented in Fig. 18. It can be seen that the ultimate moment capacities agree well using the two methods for both 500°C and 600°C. Thus it can be concluded that the proposed simplified spring connection modelling approach can be used under both ambient and elevated temperatures.

3. Performance of 2D Steel and 3D Composite Frames in Fire

Conventionally, the connections in frame simulations are usually assumed to be either rigid or pinned for ease of modelling, due to the simplicity of modelling the connections in this way. In some situations, these assumptions are made to save computational and/or time costs because the existing component based connection models require extensive computational and time costs. The simplified spring connection modelling approach proposed and validated in this research can provide an accurate and reliable way to include both the axial and the rotational ductility in frame analysis much more efficiently. In this part, two sets of investigations have been conducted to demonstrate the importance of incorporating connection axial and rotational ductility in frame analysis. A set of 2D internal steel frame models with varying beam spans, from a relatively short length (6 m) to long-span (18 m), have been studied first. These models have been chosen as continuations of the 2D isolated rugby goalpost models described earlier. A range of 3D composite frame models with increasing secondary beam spans has also been conducted to include the effect of the concrete slab and composite action and provide an insight into frame response with more realistic, ductile connection models compared with traditional rigid or pinned choices.

3.1. Influence of Connection Ductility on 2D Steel Frames

3.1.1. 2D Steel Frame Model

An internal bay of a 2D 2-storey frame has been selected to investigate the influence on frame behaviour when including connection ductility compared with conventional rigid or pinned assumptions. The beam spans vary from 6 m to 18 m to investigate the effects of the length of the beam on the ductility demands on the connections.

Fig. 19 illustrates the 2D frame and connection details adopted in this study. The bay of interest is assumed to be the middle one of a 3-bay frame, as depicted in Fig. 19(a). The beam lengths, L, vary from 6 m to 18 m in increments of 3 m. The factored uniformly distributed line load at ambient temperature is 28.9 kN/m (equivalent to a factored area load of 9.6 kN/m^2). This load gives a line load at the Fire Limit State of 18.9 kN/m and the load ratio (R) is assumed to be 0.4 for all cases. The beam sizes according to the beam span and the actual load ratio are shown in Table 1; a UC305×305×198 is selected as the column for all cases. Structural steel grade S355 is used for both the beams and the columns, with ambient temperature yield and ultimate strengths of 355 N/mm^2 and 470 N/mm^2 respectively.

For each beam span, three types of connection rigidities

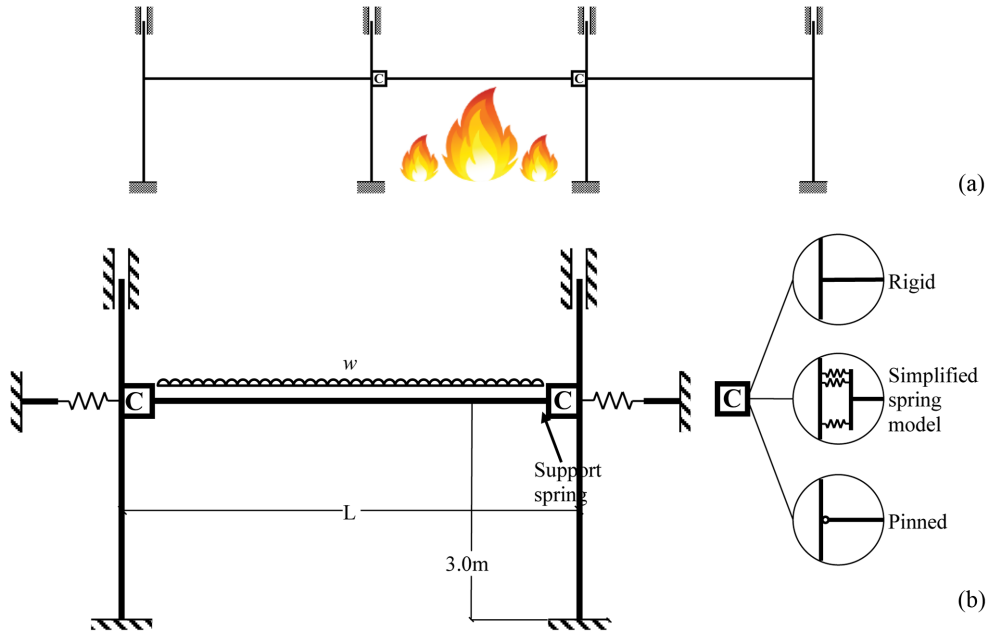


Figure 19. 2D steel frame model and connection details.

Table 1. Beam section selection

Model ID	Beam span (m)	Beam section	Actual load ratio, *R*
2D-6	6	UB305×127×42	0.39
2D-9	9	UB406×178×67	0.40
2D-12	12	UB533×210×92	0.41
2D-15	15	UB686×254×125	0.39
2D-18	18	UB762×267×147	0.43

were assigned to the beam-to-column connections: (1) rigid connection (axially and rotationally rigidly connected), (2) simplified spring connection (axially and rotationally semi-rigidly connected) and (3) pinned connection (axially rigidly connected and rotationally free).

The rigid and pinned connection cases can be achieved in *VULCAN* by amending the corresponding spring type. For the simplified spring connection case, the model developed in this research was used. The simplified spring connections were assumed to be flush endplate with design details according to SCI P398 (UK Connections Group, 2013) for each frame size as shown in Fig. 20. All endplates were in structural steel grade S275, and all bolts were property class 8.8. The same pre-processing steps were conducted according to Section 2: (1) each of the connections was divided into three T-stubs (indicated in grey dash lines in Fig. 20) followed by (2) the generation of their tensile and compressive stiffnesses using *ABAQUS*. These stiffnesses were then input into *VULCAN* as the stiffnesses of the three springs so that the simplified connections were implanted into each model.

As illustrated in Fig. 19(b), the column bases of the 2D frame are fully fixed, while the tops of the columns are only allowed to move vertically. Restraints provided by the adjacent cold structures are simulated as axial elastic springs.

The fire protection scheme adopted in this study is presented in Fig. 21. The beam is left un-protected and the temperature profile selected is flange-web-flange, where the reduction factors on the standard fire curve are 0.9-1.0-1.0. The lower columns are assumed to be protected therefore a uniform temperature distribution with a reduction factor of 0.7 on the standard fire curve is selected. The upper columns are assumed to stay at an ambient temperature of 20°C, together with the supporting structures. Since the connections are generally protected and are greater in mass due to their complex configuration compared with beams, the same temperature distribution as the lower columns is adopted.

3.1.2. Influence of Connection Ductility on 2D Steel Frames

Fig. 22 presents the axial force at the connections versus the beam temperature for various beam spans. The scales of the axes are kept consistent for ease of comparisons. Table 2 summarises the maximum axial force for the diff-

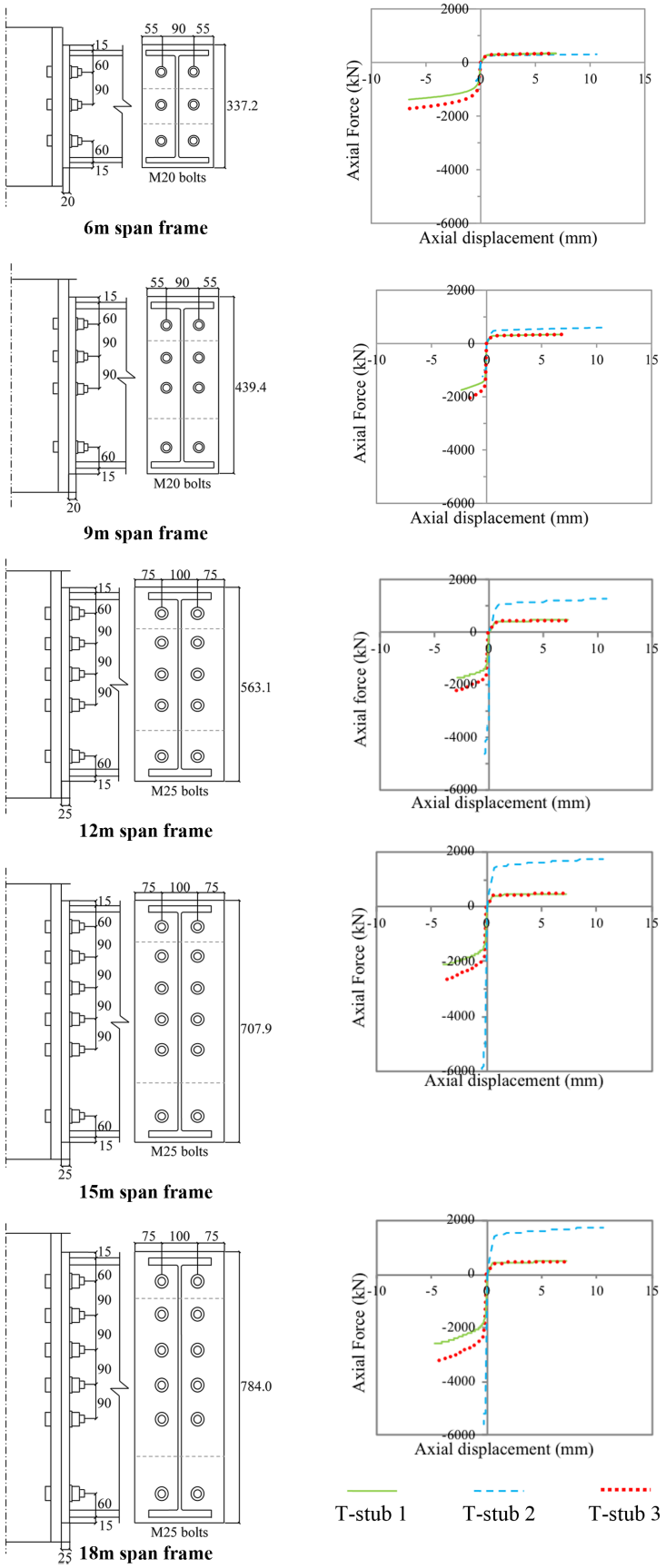


Figure 20. Flush endplate connection details and T-stub stiffnesses.

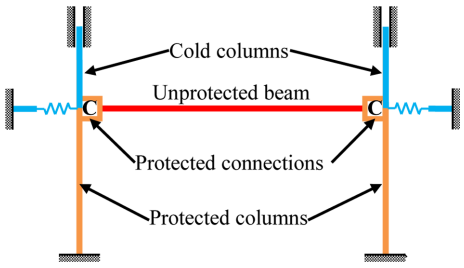


Figure 21. Fire protection scheme.

erent spans, with the axial forces in the simplified spring and the pinned connection scenarios shown both in the actual force values and in the percentage values of the axial force in the rigid connection scenario.

The axial force in the restrained beams (models with the rigid and the pinned connections in the study) usually goes through three stages in fire. With rising temperature, the axial compressive force develops and increases because of the restrained thermal expansion, with a limited amount of deflection. The ends of the beam push outwards on the connected column. During this stage, the material properties are initially elastic but degrade as the members get hotter during the fire. The axial force generated in the beam/at the connections reaches a peak compression, which is when the first stage finishes. In the second stage, the beam deflection increases which leads to a reduction in the axial compressive force in the beam. As temperature increases still further, the axial force eventually reduces to zero, which denotes the end of the second stage. In the third stage (often referred to as the catenary action stage) the axial force in the beam/at the connections enters the tensile force region resists the tensile forces resulting from the beam hanging like a cable between the two connections. The axial tensile force grows until peaking at the maximum tensile force, which is followed by a reduction in the axial tension until the end of the simulation.

When the axial ductility is included, for example by including the simplified spring connection model in this study, the axial force response changes. It can be seen from the plots that, at short spans (6 m), the axial force at the connection is almost identical for the rigid and the simplified spring connection cases, but the differences get more obvious with the increase of the beam span. The percentage values of the simplified spring connection case for different spans in Table 2 also indicate that the longer the span the greater the reduction of the axial force at the connection when spring ductility is incorporated. This finding articulates that in simulations when the connections are simply assumed to be rigid both axially and rotationally, which is common practice, the axial forces at the connection are possibly over-estimated especially for long-span structures.

Comparing the maximum axial forces for the pinned and rigid connection scenarios, the percentage values are not affected much by the span of the beam, staying between 50~55%. The reductions in the axial force at the connections are the result of the released rotational degrees of freedom in the pinned cases. The rotational flexibility permits the thermal expansion to be accommodated by thermal bowing and the compressive forces exerted on the connections by the beam are reduced dramatically. However, comparing the forces generated in the pinned and rigid cases with the values arising when simplified spring connections are used, it can be observed that the differences become smaller with increasing span. This observation leads to a deduction that in common practice simulations by simply assuming the connections to be axially restrained but rotationally free the resulting axial forces acting on the connections may be under-estimated, especially for smaller spans. For the longer span cases, the pinned connection assumptions provide similar maximum compressive force as the simplified spring connection assumptions, but the axial force responses are not as ductile.

It is indicated in Fig. 22 that the peaks of the axial force curves with the simplified spring connection cases are smoother than those of the pinned and the rigid connections cases. This variation is caused by the axial ductility that the simplified spring connection model provides. With axial flexibility in the connections, the end of the beams can move inwards or outwards when the connections experience tension or compression, closely simulating the axial ductility the connections have in reality.

3.2. Influence of Connection Ductility on 3D Composite Frames

3.2.1. 3D Composite Frame Model

The models adopted in this section consist of a typical

Table 2. Maximum axial force at the connections comparisons

Beam span (m)	Axial force in the rigid connection case (kN)	Simplified spring connection case		Pinned connection case	
		Axial force (kN)	Percentage of the rigid case (%)	Axial force (kN)	Percentage of the rigid case (%)
6	1939	1868	96	1054	55
9	3593	3339	93	1895	53
12	5153	4258	83	2688	52
15	7634	5120	67	4280	56
18	8370	6646	79	4232	51

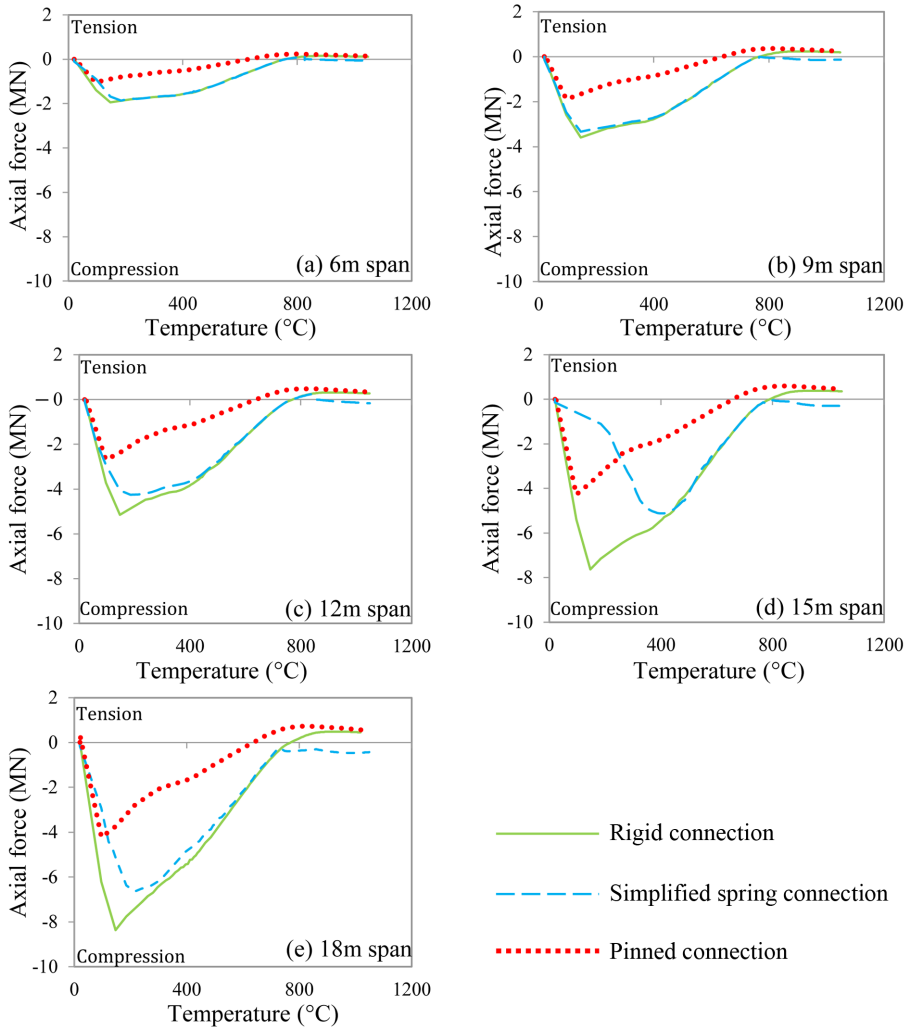


Figure 22. Axial forces at connections for various spans of the beam.

internal bay from a steel-concrete composite frame. Extra strips of composite slab, together with their downstand steel beams, located on each side of the bay are included in the models to mimic the effect of the adjacent bays. Five frame sizes are chosen for this study, and the general layout is shown in Fig. 23. The length of the primary beam (L_{prm}) is kept unchanged at 6 m while the lengths of the secondary beams (L_{sec}) are changed from 6 m to 18 m with intervals of 3 m. The design of the structural members are according to BS EN 1994-1-1 (CEN, 2005d) and BS EN 1994-1-2 (CEN, 2005e) with up to 60 minutes of fire resistance, and are shown in Table 3. For all three groups of models, other design details are kept unchanged, including: column section (UC305×305×198); height of column (3 m above and below slab panel); all steel sections are in S355; light-weight concrete with a trapezoidal profiled decking (ComFlor60 with 1.0 mm thickness); the slab was divided into 13 layers including two layers of reinforcement mesh; reinforcement mesh (A193); single shear stud per trough; permanent and variable loads 3.5 kN/m^2, resulted in a factored combined load of 9.62 kN/m^2.

The rigid and pinned connection cases can be achieved in *VULCAN* by amending the corresponding spring type. For the simplified spring connection case, the simplified spring connection model developed in this research is used. The simplified spring connections are assumed to be flush endplates and the design details according to SCI P398 (UK Connections Group, 2014) for each frame size are shown in Fig. 24. All endplates are in structural steel grade S275 and all bolts are in property class 8.8. The same pre-processing steps were conducted as for 2D frame models. The spring stiffnesses of each of the connections are also presented in Fig. 24 next to the connection details.

To reliably mimic the restraint provided by the adjacent slab panels to the bay this study is interested in, four strips of composite slabs together with their downstand steel beams are modelled as shaded in red in Fig. 25 and will be referred to as ‘slab fringes’ in this study. It needs to be highlighted that by adopting this approach the simulation results would not be as realistic as the results from modell-

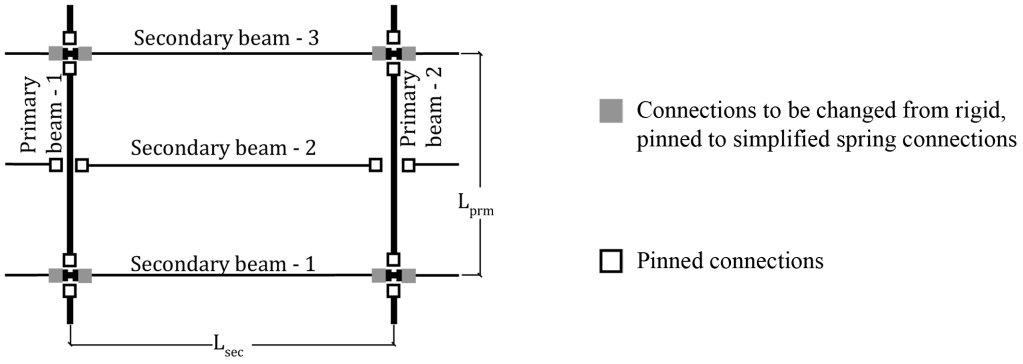


Figure 23. General floor layout.

Table 3. Beam section sizes

Model ID	Frame size	Primary beam	Secondary beam
FS1	6 m×6 m	UB356×127×33	UB254×102×25
FS2	6 m×9 m	UB457×152×82	UB305×165×54
FS3	6 m×12 m	UB457×151×74	UB457×152×82
FS4	6 m×15 m	UB610×305×179	UB533×210×122
FS5	6 m×18 m	UB762×267×197	UB686×254×140

ing all of the adjacent eight bays, however this approach is chosen for the following reasons: (a) when including the simplified spring connection models, the current version of *VULCAN* research code must have complete beams with two simplified spring connections on both ends; and (b) computational time can be significantly shortened as the number of elements is massively reduced. For the frame, the bottoms of the columns are assumed to be fully fixed while the tops of the columns are allowed to move vertically and the rotation about its longitudinal axis is restrained. For the primary beams and the edge secondary beams, out-of-plane rotations are not allowed. The intermediate secondary beam is restrained by the slab and adjacent structures. Therefore, no boundary conditions are applied. The slab elements are restrained rotationally in the vertical direction only. The downstand beam stubs labelled in Fig. 25 have the same constraints as the beam that they are a continuation of.

The assumed overall factored uniform distributed load is 9.62 kN/m^2, which is applied to the entire slab element surfaces as an area load. Conventionally, to include the loads from the adjacent bays, the primary beams would carry point loads where the intermediate secondary beams are located while the edge secondary beams would carry line loads. For this study, due to the inclusion of the slab fringes (shaded in red in Fig. 25), reductions in the point loads and the line loads are considered. The two point loads applied at the centre of the primary beams indicated as F in Fig. 26, are calculated as:

$$F = \text{Area load} \times 3\ \text{m (width of the slab panel)} \times \left(\frac{2}{3} \times \frac{1}{2} \times \text{secondary beam span}\right) \quad (1)$$

due to the width of the slab fringe was a third of half secondary beam span. Similarly, the line loads applied to the edge secondary beams indicated as UDL in Fig. 26, are calculated as:

$$\text{UDL} = \text{Area load} \times 1.5\ \text{m (width of the slab panel)} \times 1/3 = 9.62 \times 1.5 \times 1/3 = 4.81\ \text{kN/m} \quad (2)$$

as the width of the slab fringe was two-thirds of half primary beam span. For all cases, the area load (9.62 N/m^2) and the UDL (4.81 kN/m) stay unchanged while the only changing loads are the point loads due to change in the length of the secondary beams.

Similar to the 2D steel frame study, the standard fire curve is adopted for this study. The edge primary and secondary beams and the columns are assumed to be protected, and the intermediate secondary beam is left un-protected. Three types of temperature profiles for cross-sections are used: (1) top flange-web-bottom flange for the beams, (2) uniform distribution for the columns and (3) bi-linear distribution (bottom-middle-top) for the composite slabs and are presented in Table 4. Various reduction factors are applied to the standard fire temperature for each structural member to reflect their fire protection scheme (Fig. 27).

3.2.2. Influence of Connection Ductility on 3D Composite Frames

The deflections at the mid-span of the edge beam and

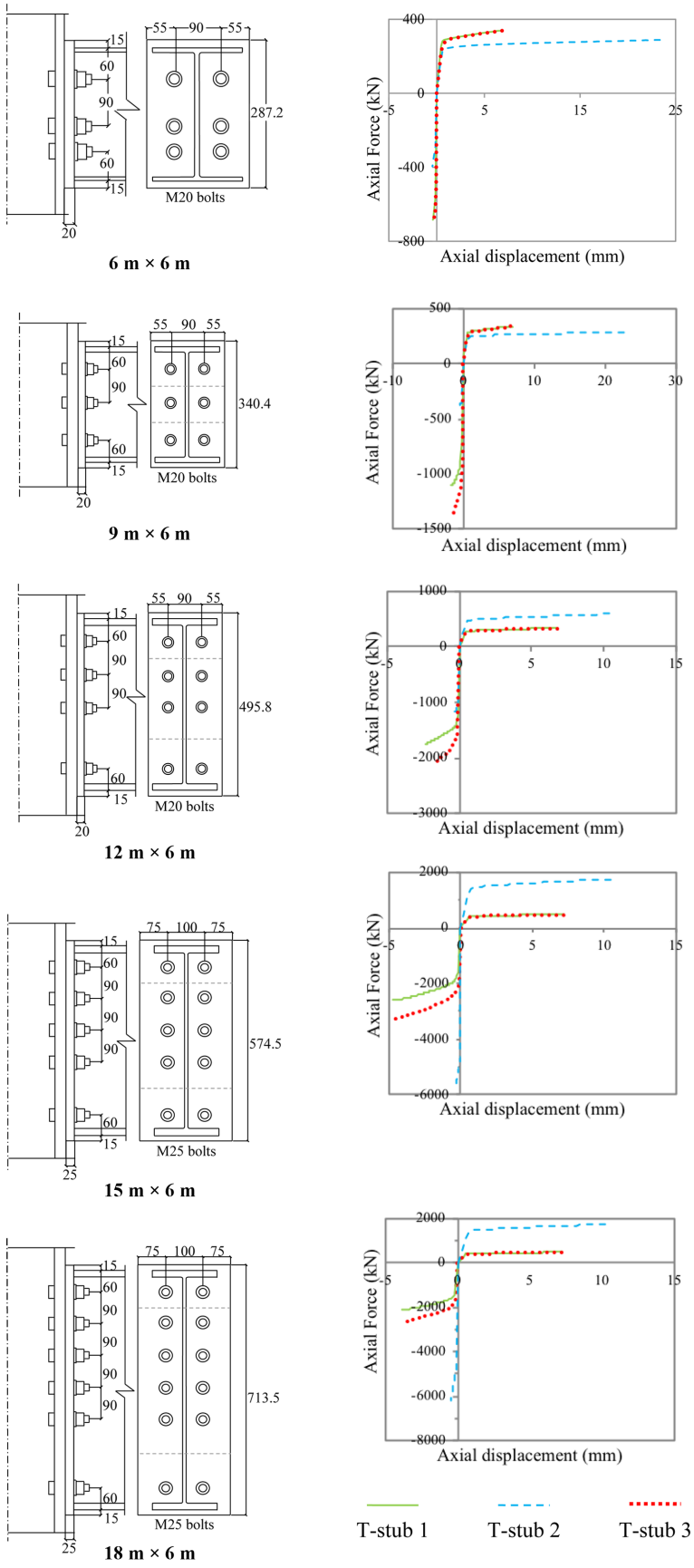


Figure 24. Flush endplate connection details and T-stub stiffnesses.

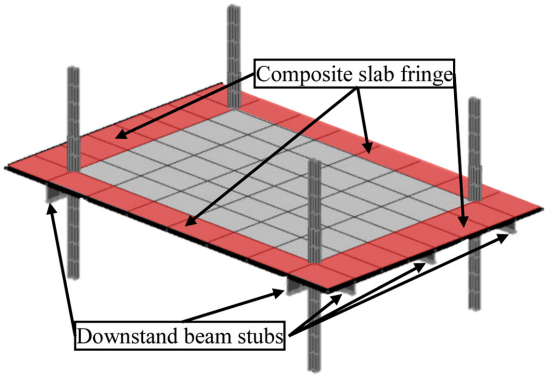


Figure 25. Composite slab strips and downstand beam stubs in the frame models.

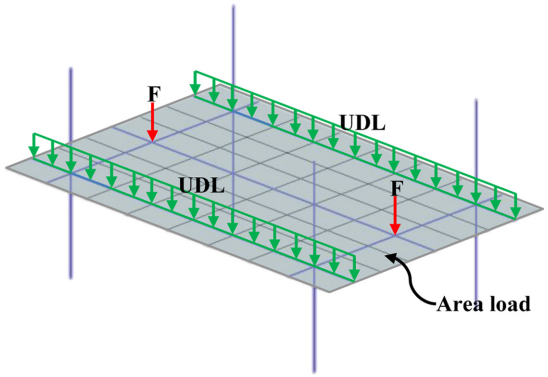


Figure 26. Loadings applied to the composite frame.

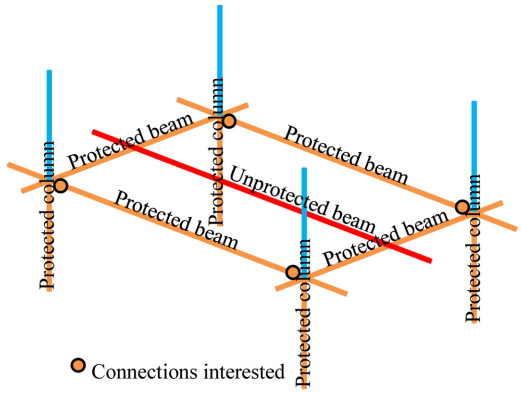


Figure 27. Steel frame protection scheme and locations of connections investigated in this study.

the slab centre, and the axial force at the connection are shown in Fig. 28. Each plot includes results from three connection types. Due to the protection scheme of the frame, following the standard fire temperature up to 120 minutes results in the temperature of the protected edge beam mid-span deflections (Fig. 28a) and the axial forces acting on the connections (Fig. 28c) being modelled up to 734°C while the slab central deflection (Fig. 28b) is modelled up to 1049°C as the intermediate secondary beam is not protected.

- Deflection

These 3D composite frame models include concrete slabs and full composite action is assumed between the slabs and the beams. At ambient temperature, since the top of the beam flanges are fully attached to the bottom surface of the slabs, the vertical deflection is restricted due to the difficulty of deforming the concrete slabs when compared with the 2D steel frame models. At elevated temperature, the existence of the composite slabs produces tensile membrane action, which stretches the central area of the slab inducing a ring of compression to reduce the vertical deflection caused by the high temperature. The deflections from the rigid connection models are always the smallest among the three connection scenarios for each frame size. This is because with the rigid connections the beam end rotation is much smaller compared with the simplified spring and the pinned connections. This limited rotation generates smaller deflections compared with the other two scenarios. On the contrary, the deflections from the simplified spring connection models are the highest among the three connection scenarios for each frame size. This is caused by the axial ductility offered by the springs at the connections compared to the axially-restrained rigid and pinned connections, where the columns provide resistance to the axial movement of the end of the beams. The plotted deflections are the combinations of the deflections in the springs and the beams.

- Axial forces acting on the connections

In 3D composite frames, the axial forces show different patterns compared with those in the 2D steel frames. Since the connections which form the focus of this study are on the slab edge secondary beams, which are protected and cooler than the un-protected intermediate secondary beam,

Table 4. Structural member temperature profile with reduction factors

Structural member	Protection	Temperature profile	Reduction factor
Primary beam	Protected	Flange – web – flange	0.6 – 0.7 – 0.7
Secondary beam (edge)	Protected	Flange – web – flange	0.6 – 0.7 – 0.7
Secondary beam (intermediate)	Un-protected	Flange – web – flange	0.9 – 1.0 – 1.0
Column (below slab)	Protected	Uniform distribution	0.7
Column (above slab)	Protected	Uniform distribution	N/A (stayed at 20°C)
Slab	N/A	Bi-linear distribution	1.0 – 0.3 – 0.2

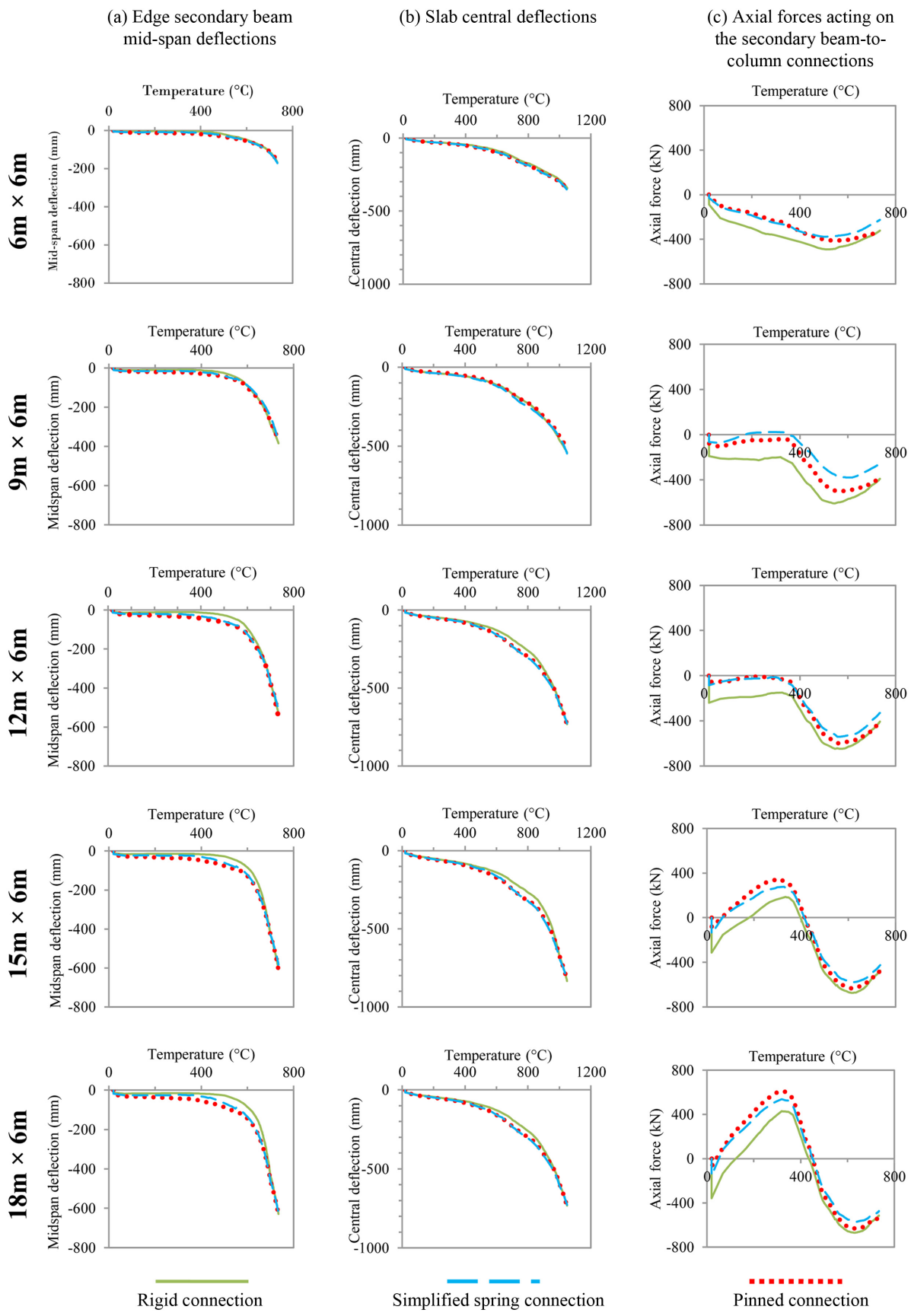


Figure 28. 3D composite frame simulation results.

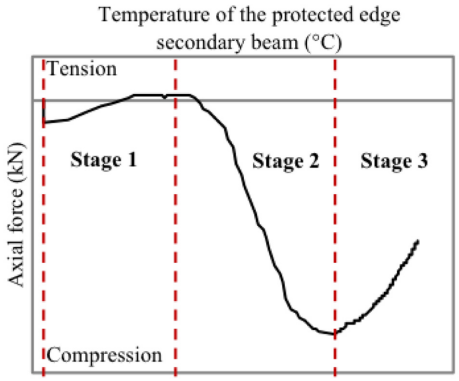


Figure 29. Typical axial force on the edge secondary beam-to-column connections in 3D composite frame.

the axial force distribution is more complex than in the 2D steel frame which has only one beam in the model. During the initial mechanical loading stage, the connections are in compression while the continuous concrete slabs on top of the connections are in tension. As temperatures increase, the axial forces acting on the edge secondary beam-to-column connections is divided into three stages as illustrated in Fig. 29 with the changes of axial force acting on the connections, ΔF_{ax}, shown in Fig. 30:

Stage 1

During the initial heating stage, thermal expansion dominates the behaviour of the frame. The intermediate secondary beam heats up faster than the edge secondary beams, resulting in the intermediate secondary beam expands faster than the edge ones. The differential expansion rates leads to the hotter intermediate secondary beam pushes the primary beam outwards together with the columns, but is restrained by the adjacent structures which are represented by the composite slab strips around the heated bay. The compression the intermediate secondary beam exerts on the primary beam reduced the axial forces acting on the secondary beam-to-column connections from the initial compressive forces induced by the mechanical loading at ambient temperature. This stage continues until the protected edge secondary beam reaches around 400°C, which is around 570°C for the un-protected intermediate secondary beam.

Stage 2

When the temperature rises further, the material degradation becomes the dominating factor, causing the beams and the slabs to become softer, which results in large rotation occurring at the interface of the beam and the column. This reflects in Fig. 30 as a dramatic increase to the peak compression, which happens around 500~550°C for the protected edge secondary beam and around 700~800°C for the un-protected intermediate secondary beam.

Stage 3

In this stage, the whole sub-frame becomes very hot. The intermediate secondary beam continues to lose its strength while the edge secondary beams start to soften, reducing the compression acting on the connections. Therefore alleviation of the axial compressive force can be observed from Fig. 30.

The axial forces acting on the connections are illustrated in Fig. 28(c). It can be seen that by including the axial and rotational ductility of the connections into the 3D composite structure modelling the peak compressive forces acting on the connections are less than the conventional rigid or pinned connection assumptions. Within each frame size, it can be seen that the models with rigid connections suffer the highest compressive forces. This is as expected since the rigid connection assumption essentially stops the beam from any form of movement from the column flanges, the axially restrained beam end generates high axial forces acting on the connections. Similarly, the pinned connection assumption only frees the rotational degrees of freedom and brings only limited reductions in the axial forces acting on the connections. With the more realistic simplified spring connection model which allows ductility

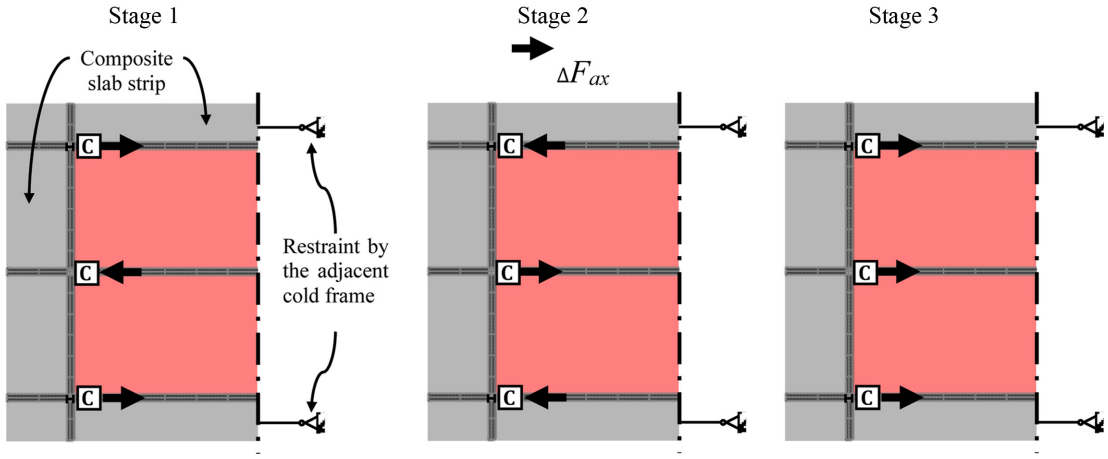


Figure 30. Typical changes in axial force, ΔF_{ax}, acting on connections.

Table 5. Maximum axial force at the connections comparisons

Frame size	Rigid connection case (kN)	Pinned connection case (kN)	Simplified spring connection case		
			Axial force (kN)	Percentage of the rigid case (%)	Percentage of the pinned case (%)
6 m × 6 m	490	413	378	77	92
6 m × 9 m	609	504	380	62	75
6 m × 12 m	648	600	542	84	90
6 m × 15 m	673	633	577	86	91
6 m × 18 m	670	632	571	85	90

both axially and rotationally, the reductions are more obvious. Table 5 provides a quantitative comparison of the maximum axial forces in the form of the actual values and as percentages of the highest case. By including the axial and rotational ductility in the 3D composite frame simulations, the maximum axial forces acting on the connections are lower than the rigid connection assumption. The included axial ductility allows the beam end to move without pulling or pushing the column flanges directly, but instead by deforming the connections. Once again it shows that by using the conventional connection assumptions, which ignore the axial and rotational ductility of the connections, the maximum axial forces acting on the connections are overestimated. The misrepresentation of the actual behaviour of the connections under fire conditions can lead to over designing structural members and an increase in costs.

4. Discussion & Conclusion

This research has developed a simplified spring connection modelling approach for steel flush endplate beam-to-column connections, which can be used in 2D steel or 3D composite frame analysis under elevated temperature. Connections are dismantled into two or three T-stubs, depending on their geometrical configurations, and the force-displacement characteristic of each T-stub is generated in *ABAQUS* through detailed finite element modelling. The generated force-displacement curves are then input into *VULCAN*, with corresponding lever arms to form the spring connection model. The axial and rotational ductilities can be represented by the sum or the difference of the springs. The proposed simplified spring connection model has been implemented into *VULCAN* and has been validated against both the same spring connection model in *ABAQUS* and against isolated tests.

The pre-processing procedure requires a considerable amount of computation and time, significantly prolonging the frame simulation when the proposed simplified spring connection model is adopted. The detailed T-stub models in *ABAQUS* are created based on the geometrical configurations and the material properties of the T-stubs, together with the contact elements between each two T-stub components (beam flange and web, endplate, column flange and bolt assemblies). This pre-processing time can be shortened if the relationship of the tensile and compressive characteristics of similar T-stub assemblies can be quantified.

Currently, frame analysis with multiple connections is difficult to conduct with the available connection modelling approach – detailed component based method – due to the high demand of computation and time. Connections in frame analyses are usually assumed to be either rigid or pinned, ignoring the axial and/or rotational ductility the connections may possess. The proposed simplified connection model enables the inclusion of more realistic steel beam-to-column connection behaviour in frame analyses.

Although flush endplate connections were the focus of this research, there is a possibility for the proposed approach to be adapted to model other connections types, subject to further validations.

In this research, the influences of connection ductilities on frame behaviour in fire were investigated through simulations on a series of 2D steel and 3D composite internal sub-frames with the secondary beam-to-column connections modelled as rigid, pinned or using the proposed simplified spring connection model. The spans of beam varied from 6 m to 18 m for the 2D steel frame models and 6 m to 12 m for the 3D composite frame models. The models were assigned realistic loading conditions and temperature distributions.

In the 2D steel frames, generally the restrained steel beam goes through three stages with increasing temperature: (1) retrained thermal expansion induces axial compressive forces acting on the connections and reaches a maximum value; (2) the axial compressive force then reduces due to material degradation under elevated temperature and (3) the axial forces acting on the connections become net tensile due to the beam loss of strength causing it to hang cable-like between the two connections. It was observed from the 2D steel frame analyses that, the axial forces acting on the connections were overestimated when assuming the connections to be rigid, and were under-estimated by assuming the connections to be pinned. It is shown that these two conventional assumptions cannot represent the behaviour of the frames in fire accurately.

The change in axial force acting on the connections in the 3D composite frame is much more complex due to the involvement of the composite slab, the temperature differences in the members and the complicated restraint aris-

ing from the surrounding cold structural members. The axial force acting on the critical edge secondary beam-to-column connections generally goes through three stages in fire: (1) axial compressive force induced by the initial mechanical loading at ambient temperature is reduced because of the differential expansion rate of the un-protected internal and protected edge secondary beams, the intermediate secondary beam pushes the primary beam outwards; (2) the axial compressive force then increases dramatically since the un-protected intermediate secondary beam starts to lose its strength in fire, pulling the primary beam inwards; and (3) the axial compressive force is reduced again as the protected edge secondary beams begin to lose their strength significantly. It was found that by assuming the connections to be rigid or pinned, the vertical deflections at the centre of the slab and the mid-span of the edge secondary beams were not affected significantly. However, influences of the connection ductility were shown in the axial forces acting on the secondary beam-to-column connections. Compared with the results from the model using the proposed simplified spring connection, by assuming these connections to be rigid, the axial forces acting on them are over-estimated; by assuming them to be pinned, the axial forces acting on them are similar up to the end of Stage 2, but smaller peak axial forces were observed.

The above results emphasize the importance of including connection axial and rotational ductility in frame analysis at elevated temperature so that more realistic frame response can be predicted for performance based fire engineering.

References

BSI (1981) BS 3643-1:1981 Specification for ISO Metric Screw Threads - Part 1: Principles and Basic Data. 1981 ed. British Standards Institution, London, UK.

BSI (2013) BS EN ISO 898-1:2013, Mechanical properties of fasteners made of carbon steel and alloy steel. British Standards Institution, London, UK.

Burgess, I.W., Davison, J.B., Huang, S.-S. & Dong, G. (2012). "The Role of Connections in the Response of Steel Frames to Fire." Structural Engineering International, 22(4), 449-461.

CEN (2005a) EN 1993-1-1 Eurocode 3: Design of steel structures: Part 1-1: General rules. European Committee for Standardisation, Brussels, Belgium.

CEN (2005b) EN 1993-1-2 Eurocode 3: Design of Steel Structures: Part 1-2 Structral Fire. European Committee for Standardisation, Brussels, Belgium.

CEN (2005c) BS EN 1994-1-1:2004 Design of composite steel and concrete structures: Part 1-1: General rules and rules for buildings. BritishStandards Institution, London, UK.

CEN (2005d) BS EN 1994-1-2:2004 Design of composite steel and concrete structres: Part 1-2: General rules — Structural fire design. British Standards Institution, London, UK.

FEMA (2002a) World Trade Centre Building Performance Study. Federal Emergency Management Agency, USA.

FEMA (2002b) World Trade Centre Building Performance Study: Data Collection, Preliminary Observations, and Recommendations. Federal Emergency Management Agency, USA.

ISO (1999) ISO 834-1:1999 Fire-resistance tests - Elements of building construction. General requirements. International Standards Organisation, Geneva, Switzerland.

Newman, G. M., Robinson, J. T. & Bailey, C. G. (2006) Fire safety design: a new approach to multi-storey steel framed building. The Steel Construction Institute, London, UK.

Simões da Silva, L., R. O. de Lima, L., C. G. da S. Vellasco, P. and A. L. de Andrade, S. (2004) "Behaviour of flush endplate beam-to-column joints under bendng and axial force." Steel and Composite Structures, 24, 77-94.

Sun, R.R., Burgess, I. W., Huang, Z.-H. & Dong, G. (2015) "Progressive failure modelling and ductility demand of steel beam-to-column connections in fire." Engineering Structures, 89, 66~78.

UK Connections Group (2013) Joints in steel construction: Moment-Resisting Joints to Eurocode 3. BCSA & SCI, UK.